Modelling the growth stress in tree branches: impact of different growth strategies

A van Rooij, Eric Badel, Jean-François Barczi, Yves Caraglio, Tancrede Almeras, Joseph Gril

Modelling the growth stress in tree branches: impact of different growth strategies

A. Van Rooij[1,2], E. Badel[2], J.F. Barczi[3], Y. Caraglio[3], T. Alméras[4] and J. Gril[1,2]

1. Université Clermont-Auvergne, CNRS, Institut Pascal, F-63000, Clermont-Ferrand, France
2. Université Clermont-Auvergne, INRAE, PIAF, F-63000, Clermont-Ferrand, France
3. CIRAD, Unité Mixte de Recherche (UMR) Cirad-Cnrs-Inra-Ird-Université Montpellier 2, 'botAnique et bioinforMatique de l'Architecture des Plantes' (AMAP), A-51/PS2, Boulevard de la Lironde, 34398 Montpellier cedex 5, France
4. LMGC, CNRS, Université of Montpellier, Montpellier, France

Abstract

This work aims to model the mechanical consequences of different strategies used by tree branches to ensure their posture despite the increasing loading due to gravity. The two known strategies of a branch to straighten itself are the asymmetry of maturation stress, including reaction wood formation, and eccentric growth. Both strategies can be observed in nature and influence the stress distribution developed in the branch each year. This so-called growth stress reflects the mechanical state of the branch. In this work, a growth stress model was developed at the cross-section level in order to quantify the bio-mechanical impact of each strategy. For illustration, this model was applied to the branches of two 50-year-old trees, one softwood *Pinus pinaster* and one hardwood *Prunus avium*, both simulated with the AMAPSim finite element software. The model show that in hardwoods, both strategies are efficient and that the combination of the two is optimal. In softwoods, the model shows that eccentricity process is less efficient. Moreover, eccentricity process does not necessarily act as a relevant lever for postural control. However eccentricity process greatly modify the profile pattern of mechanic stress. This work opens exciting experimental perspectives in order to understand the biomechanical process involved in the building of branches.

Abbreviations and notations (in order of occurrence)

NW,TW,CW	Normal Wood, Tension Wood, Compression Wood
(x, y, z)	Local reference system associated with the section
O	Centre of the section
r, R	Radii of the cross section (m)
$e(R), \overline{e(R)}$	Eccentricity at the stem radius R, integrated eccentricity up to r = R
(x', y', z')	Local reference system associated with the section, centred on the pith
σ	Stress (MPa)
σ_0	Induced maturation stress (Mpa)
S	Cross section area (m^2)
N, M	Loads (N): normal force parallel to z' and bending moment around y'
E	Module of elasticity in L direction (GPa): MOE
μ	Induced maturation strain
ϵ, a, b	Deformations: strain at the center, changes in curvature around x,y
K_i	Structural stiffness of the cross-section
F_i	External coefficients (maturation and load)
θ	Circumferential position in section (rad)
$\sigma_0(\theta)$	Maturation strain in the new ring at circumferential position θ
α	Mean maturation stress in the new ring
β	Differential stress in the new ring
$r_{x'y'}$	Radius of the cross section at the instant of appearance of the point (x', y')
$\lambda_N, \lambda_M, \nu_M, \nu_N$	Load power law: allometric coefficient
λ_b, ν_b	Change of curvature power law: allometric coefficient
$\sigma_{NW}, \sigma_{TW}, \sigma_{CW}$	Maturation stress in the normal wood, tension wood and compression wood
$\overrightarrow{N_n}, \overrightarrow{M_n}$	Loads of growth unit n: normal force and bending moment around y
N_z, M_x, M_y, M_z	Loads of growth unit n: projection of $\overrightarrow{N_n}$ on $\vec{z}$ and bending moment $\overrightarrow{M_n}$ around $\vec{x}, \vec{y}, \vec{z}$
m_n	Mass of the growth unit n (kg)
g	Acceleration of gravity: $g = 9.8$ m.s^{-2}
G_n	Centre of gravity of the growth unit n
E_d, E_g	Green, air-dry MOE
ρ	Density
$\mu_{NW}, \mu_{TW}, \mu_{CW}$	Maturation strain in the normal wood, tension wood and compression wood
μstrain	$1/10^6$
D_n, D_{n+1}	First and second diameter the growth unit n
D	Deflection of a growth unit
L_n	Length of the growth unit n

Introduction

From a mechanical point of view, wood in tree fulfils three major functions: construction of the architecture, postural maintenance and resistance to external elements [Thibaut (2019)]. These three functions are provided by the way wood cells differentiate and accumulate. Each axis of a tree can be considered as an inclined beam, consisting of a succession of conical growth units [Barthélémy and Caraglio (2007)]. It is built in two steps: primary growth resulting in new growth units that increase the length of the axis; secondary growth resulting in thickening of already existing units by addition of annual rings. These two interactive and additional processes lead to a specific pattern of mechanical stress, called 'growth stress', superposition of support stress and maturation stress [Archer (1976); Fournier et al. (1991a)]. The support stress results from the continuous increase of the weight supported by the axis over the years. It vanishes near stem periphery where the recently formed wood contributes to the support of recently produced biomass only, and reaches maximal levels in the core of the stem. Maturation stress is set up at the end of the cell-wall maturation process, when molecular components such as lignin polymerise, generating growth forces by small dilatation or contraction restrained by the rigidity of the previously formed wood cells [Alméras and Clair (2016)]. An evaluation of the maturation stress can be obtained by measuring the strain associated to stress release at stem periphery, where no support stress is present [Nicholson (1971); Yoshida and Okuyama: (2002); Yang et al. (2005)]. The circumferential heterogeneity of this peripheral stress is needed to regulate stem curvature. In most cases, a tensile maturation stress is produced in the newly formed 'normal wood' (NW). But observations on inclined trunks [Alméras et al. (2005); Coutand et al. (2007); Thibaut and Gril (2021)], seedlings [Hung et al. (2016)] and branches [Fisher and Stevenson (1981); Huang et al. (2010); Tsai et al. (2012); Hung et al. (2017)] have evidenced a clear difference between hardwoods and softwoods trees. Hardwoods are able to produce 'tension wood' (TW) inducing a much higher tensile stress on one side, while for softwood a compressive stress is induced in 'compression wood' (CW). The first pulls, the second pushes. In the most usual case of an inclined stem restoring vertical orientation, TW is formed on the upper side and CW on the lower; but other situations can be encountered depending on the biomechanical requirements of the tree [Wang et al. (2009)]. In addition to their participation in the postural control of tree stems, these two types of so-called 'reaction wood' (RW) are characterised by a different anatomy (not discussed here) and specific physical and mechanical properties.

Growth stress modelling plays an important role in the understanding of the phenomena involved in the orientation process of a stem. The history of biomechanical models begins with Kübler (1959) who proposed an analytical formulation of growth stress for a perfect cylinder made of a homogeneous and transversally isotropic wood. Later, Archer and Byrnes (1974) took into account an asymmetry of the maturation stresses, and Fournier et al. (1991a,b) proposed a semi-incremental version of these models, allowing to take into account a potential gradient of mechanical parameters (stiffness, maturation). By associating their previous model to the loading induced by the tree weight, Fournier et al. (1994) made the connection between growth stress and stem orientation. To understand the parameters involved in orientation of the stems, this model has been taken up and developed by several authors. Yamamoto et al. (2002) added a primary shoot and went back to curvature calculations. Alméras and Fournier (2009) introduced the notion of gravitropic performance (capacity of the tree to correct the bending moment induced by its weight) and gave criteria of long-term stability. Huang et al. (2005) and Alméras et al. (2005) also made the model more realistic by introducing the pith eccentricity and by introducing spatial heterogeneity of stiffness, which allowed them to quantify the effectiveness of eccentricity, maturation, stiffness gradient and inital radius in the curvature correction process. They both showed that the main factor in the gravitropic correction process is the distribution of the maturation stresses. Still in line with Fournier's 1994 model, Alméras et al. (2018) recently developed analytical models of longitudinal growth stresses, taking into account different configurations, like eccentricity or maturation gradient, and evolution laws, like evolution of stiffness per additional layer. Finally, based on the same philosophy as that established by Kübler, tree-scale and finite-element models have emerged [Fourcaud et al. (2003); Ancelin et al. (2004)].

Most of these models have been applied to trunks. Some theoretical predictions have been made on inclined trunks [Alméras and Fournier (2009)] and only one analytical work has been done so far on branches [Huang et al. (2010)]. Branches are particular axes subject to large inclinations, and some assumptions such as uniformity of eccentricity find their limits. The only model proposing an integration of the stress on the whole section, proposed by Fourcaud et al. (2003), did not take into account the eccentricity at all. Huang et al. (2005) and Alméras et al. (2005) have quantified the roles of maturation and eccentricity in the recovery process, but have not evaluated their ability to ensure an imposed growth scenario.
In this framework, we propose a semi-incremental biomechanical model of growth stress at the cross section

level that takes into account the eccentricity and maturation gradients during the building of branches. Using the digital models of a hardwood and a softwood, the impact of each of these two straightening strategies on the stress state will be evaluated

Material and methods

Numerical model

General hypotheses

The problem will is set in the framework of beam theory. From a geometrical point of view, branches generally show profiles that are well suited to this type of analytical framework: slender shape, no important diameter variations. The shape effects due to twigs and other local biological phenomena (cavity, nodes, etc.) are neglected. The same set of hypotheses as in Alméras et al. (2018) is adopted. In this study, we focus on the behaviour in the longitudinal direction (parallel to the main axis). Horizontal bending and torsion loads are not considered. Only the vertical bending moment (that caused by the weight) is considered. These initial hypotheses on the loading modes will be discussed later.

Geometrical settings

The object of study is the cross-section of a branch, placed within a plane locally orthogonal to the pith. The local reference frame of the section is $(\vec{x}, \vec{y}, \vec{z})$, with $\vec{z}$ the longitudinal direction of the axis, and $\vec{x}$ placed in a vertical plane and facing upwards (Figure 1). The shape of the cross-section is assumed to be circular at any stage of development, described by the successive deposition of wood rings. The term of 'ring' refers here to the volume occupied by wood cells produced by the cambium during a certain duration of time, not necessarily annual: it must be taken in a numerical sense. These rings possibly present an eccentricity resulting from asymmetry of secondary growth. Since the model only takes into account vertical bending, the eccentricity is set along the x axis, as expressed by the following equation:

$$O(t) = \int_0^{R(t)} e(r)dr = \bar{e}R(t) \tag{1}$$

with $O(t)$ the position of the geometrical centre and $R(t)$ the radius of the section at time t, e(r) the eccentricity when the stem radius was r and $\bar{e}$ the integrated eccentricity up to $r = R$. The eccentricity varies in the interval $[-1, 1]$. A zero eccentricity corresponds to a centred section, while -1 or 1 corresponds to maximum eccentricity resulting from secondary growth only on the lower or the upper side of the section, respectively. In the following, the position x' in the pith reference frame will be needed. By calling x the vertical position in the geometrical reference frame, we deduce from equation 1:

$$x = x' - \bar{e}R \tag{2}$$

Computation of the mechanical behaviour

We will develop a radial incremental method. For each radial increment, the longitudinal stress is computed so as to satisfy the static equilibrium of the cross section:

$$\begin{cases} \int_S \delta\sigma dS + \int_{\delta S} \sigma_0 dS = \delta N & \text{(3a)} \\ \int_S \delta\sigma x dS + \int_{\delta S} \sigma_0 x dS = -\delta M & \text{(3b)} \end{cases}$$

where S is the cross-section and δS its increment, $\delta\sigma$ the increment of stress σ in the already formed wood, in response to the maturation stress σ_0 generated in the new wood layer, δN and δM the increment of external force N and bending moment M, respectively, applied on the cross-section. For illustration, the geometric situation for K rings and an increment of stem radius δR is proposed in Figure 1.

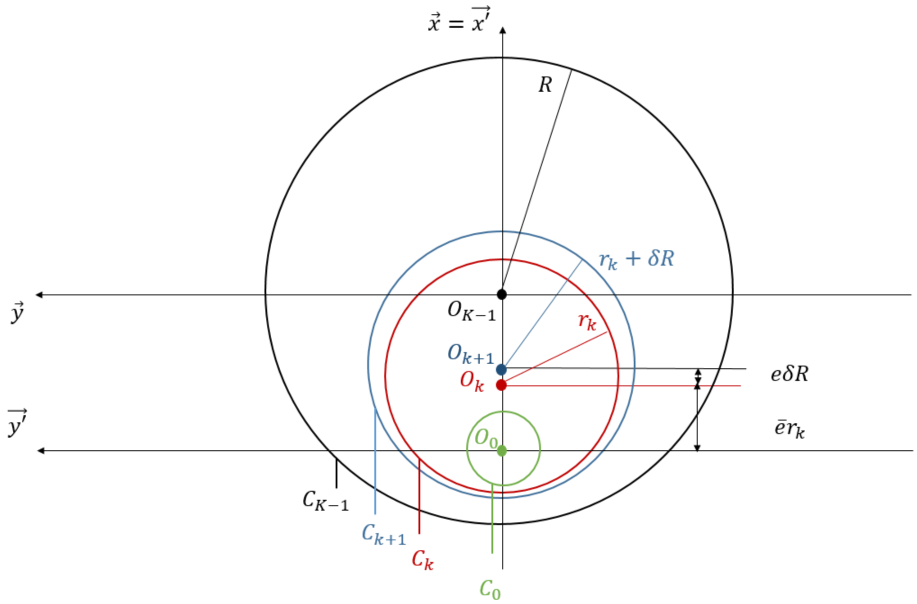

Figure 1: Geometrical representation of a section with K numerical rings and a radial increment δR between rings $k-1$ and k.

The stress σ is linked to the strain ϵ by a pre-stressed Hooke law:

$$\sigma = E\left(\epsilon - \mu\right) = E\epsilon + \sigma_0 \tag{4}$$

with E the longitudinal Young's modulus, μ the maturation strain and σ_0 the maturation stress. In the context of the beam theory, the planar sections remain planar sections (Euler-Bernouilli assumption), so that the strain field is described by the deformation a at the centre of the pith and the curvature b relative to the y-axis:

$$\delta\epsilon = \delta a + x\delta b \tag{5}$$

where $\delta\epsilon$, δa, δb are the increments of ϵ, a, b, respectively. The stress increment $\delta\sigma$, in the already formed wood where no maturation occurs anymore, can then be deduced:

$$\delta\sigma = E\delta\epsilon = E(\delta a + x\delta b) \tag{6}$$

From these considerations, the system (3) becomes (details of the calculation are given in Appendix A):

$$\begin{cases} K_0\delta a + K_1\delta b = \delta F_0 & \text{(7a)} \\ K_1\delta a + K_2\delta b = \delta F_1 & \text{(7b)} \end{cases}$$

with

$$K_0 = E\pi R^2, \quad K_1 = E\pi\bar{e}R^3, \quad K_2 = E\pi R^4\left(\bar{e}^2 + \frac{1}{4}\right) \tag{8}$$

$$\delta F_0 = -\int_{\delta S}\sigma_0 dS + \delta N, \quad \delta F_1 = -\int_{\delta S}\sigma_0 x dS - \delta M$$

The calculation of the coefficients δF_0 and δF_1 depends on the formulation of the maturation stress. The maturation stress is assumed to vary circumferentially as follows:

$$\sigma_0(\theta) = \alpha + \beta\cos\theta \tag{9}$$

where the mean stress α and differential stress β are defined differently in softwood and hardwood species:

$$\begin{cases} \text{Hardwood: } \alpha = \dfrac{\sigma_{TW} + \sigma_{NW}}{2}; \beta = \dfrac{\sigma_{TW} - \sigma_{NW}}{2} & (10a) \\ \text{Softwood: } \alpha = \dfrac{\sigma_{CW} + \sigma_{NW}}{2}; \beta = \dfrac{\sigma_{NW} - \sigma_{CW}}{2} & (10b) \end{cases}$$

with σ_{TW} (resp. σ_{CW}) the maturation stress in the tension wood (resp. compression wood), and σ_{NW} the stress in the opposite wood (normal wood). One gets :

$$\begin{cases} \delta F_0 = -\pi R \left(2\alpha + e\beta\right) \delta R + \delta N & (11a) \\ \delta F_1 = -\pi R^2 \left(3\alpha e + e^2\beta + \beta\right) \delta R - \delta M & (11b) \end{cases}$$

From equations (8), (11a) and (11b), the components of the system (7) are known. By inversion, $\delta\alpha$ and δb can be obtained (see details in Appendix B):

$$\begin{cases} \delta a = \dfrac{4}{ER}\left[\left(3e\bar{e} - 2e^2 - \dfrac{1}{2}\right)\alpha + \left(\bar{e}e^2 - e\bar{e}^2 + \bar{e} - \dfrac{e}{4}\right)\beta\right]\delta R + \dfrac{4}{E\pi R^3}\left[\bar{e}\delta M + \left(\bar{e}^2 + \dfrac{1}{4}\right)R\delta N\right] & (12a) \\ \delta b = \dfrac{-4}{ER^2}\left[\left(3e - 2\bar{e}\right)\alpha + \left(e^2 - e\bar{e} + 1\right)\beta)\right]\delta R - \dfrac{4}{E\pi R^4}\left(\delta M + \bar{e}R\delta N\right) & (12b) \end{cases}$$

Once δa and δb are known, the stress increment $\delta\sigma$ at any position given by (x', y') can be obtained from (6). The stress distribution at this position can be obtained as the sum of the initial maturation stress and all the stress increments undergone by the material point since its creation.

$$\sigma(x', y', R) = \sigma_0(x', y') + \sum_{k=k_{x'y'}}^{K} \delta\sigma_k \tag{13}$$

where $\delta R_k = r_k - r_{k-1}$ for a succession of ring radii $r_0 = 0 < r_0 < ... < r_k < ... < r_K = R$, $\delta\sigma_k$ is the corresponding increment, and $k_{x'y'}$ designates the ring containing the point.

Analytical formulations

When each incremental term in expression (12b) is divided by dR and dR tends to zero, the ratio tends to the derivative against R, leading to :

$$\begin{cases} \dfrac{\mathrm{d}a}{\mathrm{d}R} = \dfrac{4}{ER}\left[\left(3e\bar{e} - 2e^2 - \dfrac{1}{2}\right)\alpha + \left(\bar{e}e^2 - e\bar{e}^2 + \bar{e} - \dfrac{e}{4}\right)\beta + \dfrac{1}{\pi R^2}\left(\bar{e}\dfrac{\mathrm{d}M}{\mathrm{d}R} + \left(\bar{e}^2 + \dfrac{1}{4}\right)R\dfrac{\mathrm{d}N}{\mathrm{d}R}\right)\right] & (14a) \\ \dfrac{\mathrm{d}b}{\mathrm{d}R} = \dfrac{-4}{ER^2}\left[\left(3e - 2\bar{e}\right)\alpha + \left(e^2 - e\bar{e} + 1\right)\beta + \dfrac{1}{\pi R^2}\left(\dfrac{\mathrm{d}M}{\mathrm{d}R} + \bar{e}R\dfrac{\mathrm{d}N}{\mathrm{d}R}\right)\right] & (14b) \end{cases}$$

If the division by δR is applied to the stress σ, a function of the stem radius R and the position x', the partial derivative $\partial\sigma/\partial R$ is obtained, so that equation (13) becomes:

$$\sigma(x', y', R) = \sigma_0(x', y') + \int_{r_{x'y'}}^{R} \frac{\partial\sigma}{\partial R}(x', R')dR' \tag{15}$$

by calling $r_{x'y'}$ the radius of the section at the instant of appearance of the point with coordinates (x', y').

The expressions of axial force $N(R)$ and bending moment $M(R)$ are needed to compute the evolution of the stress distribution in the cross section. For this purpose, we assume that they vary as a power function of the radius. This results in the following allometric laws:

$$\begin{cases} N = \lambda_N R^{\nu_N} & (16a) \\ M = \lambda_M R^{\nu_M} & (16b) \end{cases}$$

with $\lambda_{N,M}$ and $\nu_{N,M}$ allometric coefficients. The $\lambda-$coefficients are directly proportional to the weight supported by the cross section, either that of the branch itself or that of axes of higher orders. The $\nu-$coefficients express the kinetics of the secondary growth: a small ν refers to an early secondary growth, a higher one to a later diameter increase.

The calculation of σ requires also the knowledge of the curvature rate $\frac{\mathrm{d}b}{\mathrm{d}r}$. In most of the cases we will assume the stationarity of the branch orientation. This results in $\frac{\mathrm{d}b}{\mathrm{d}r} = 0$ and the fact that the branch balances its weight increment at every deposition of a new wood layer. However, we can consider two cases for which the branch does not build up in a stationary way: passive bending (under its own weight), and up-righting (the action of maturation is stronger than the additional weight). In both cases, the change in curvature has been calculated by Alméras and Fournier (2009) and Alméras et al. (2018) as follows:

$$\begin{cases} \text{Up-righting:} & \frac{\mathrm{d}b}{\mathrm{d}r} = -4\frac{\beta}{Er^2} & (17a) \\ \text{Passive bending:} & \frac{\mathrm{d}b}{\mathrm{d}r} = 4\frac{\lambda_M \nu_M}{E\pi} r^{\nu_M - 5} & (17b) \end{cases}$$

For the calculation, we will then take a general law:

$$\frac{\mathrm{d}b}{\mathrm{d}r} = \lambda_b r^{\nu_b} \tag{18}$$

Combining (14),(15),(16) and (18), the total stress can then be computed as:

$$\sigma^i(x', y', R) = \sigma_0^i(x', y') + S_1 \ln\left(\frac{R}{r_{x'y'}}\right) + \frac{S_2}{S_3}\left(R^{S_2} - r_{x'y'}^{S_2}\right) + \frac{S_4}{S_5}\left(R^{S_5} - r_{x'y'}^{S_5}\right) + \frac{S_6}{S_7}\left(R^{S_7} - r_{x'y'}^{S_7}\right) x' \tag{19}$$

where $S_1 = 4\left[\left(3e\overline{e} - 2e^2 - \frac{1}{2}\right)\alpha + \left(\overline{e}e^2 - e\overline{e}^2 + \overline{e} - \frac{e}{4}\right)\beta\right]$ is driven by the maturation process, $S_2 = \frac{\lambda_N \nu_N}{\pi}\left(\overline{e}^2 + \frac{1}{4}\right)$, $S_3 = \nu_N - 2$, $S_4 = \frac{4}{\pi}\lambda_M \nu_M \overline{e}$ and $S_5 = \nu_M - 3$ by branch loading (geometric evolution of the branch), $S_6 = E\lambda_b$ and $S_7 = \nu_b + 1$ by the orientation of the branch.
For each radius r, the remaining unknowns are the mean stress α, the differential stress β and the eccentricity e. Equation (14b) can be rewritten as:

$$(3e - 2\overline{e})\,\alpha + \left(e^2 - e\overline{e} + 1\right)\beta = \frac{-1}{\pi r^2}\left(\frac{dM}{dR} + \overline{e}R\frac{dN}{dR}\right) - E\frac{R^2}{4}\frac{db}{dR} \tag{20}$$

Thus by fixing two parameters, the third is directly determined. The maturation parameters α and β being determined by the maturation stress in normal wood σ_{NW} and reaction wood σ_{TW} or σ_{CW} according to (10), these parameters will be managed.
We will consider two possible configurations for the simulations in next section:

1. First, we apply a constant eccentricity (so that $\bar{e} = e$) and we fix the stress level in the normal wood. In that case, the maturation stress of the reaction wood is given by equations (10):

$$\begin{cases} \sigma_{TW} = \dfrac{-2}{\pi r^2(1+e)} \left(\dfrac{dM}{dr} + er\dfrac{dN}{dr} \right) + \sigma_{NW} \left(\dfrac{1-e}{1+e} \right) + \lambda_b \left(\dfrac{Er^2}{2(1+e)} \right) r^{\nu_b} & \text{(21a)} \\ \sigma_{CW} = \dfrac{2}{\pi r^2(1-e)} \left(\dfrac{dM}{dr} + eR\dfrac{dN}{dr} \right) + \sigma_{NW} \left(\dfrac{1+e}{1-e} \right) - \lambda_b \left(\dfrac{Er^2}{2(1-e)} \right) r^{\nu_b} & \text{(21b)} \end{cases}$$

2. Second, we fix the maturation parameters and we observe how the branch straighten, or not, just by varying the eccentricity of the secondary growth. In this configuration, equation 14b becomes a two degree equation in e that can be solved numerically.

In these two configurations, using data on the support allometries $\lambda_N, \lambda_M, \nu_M, \nu_N$ we can calculate the stress in the reaction wood and/or the eccentricity with different (λ_b, ν_b), then deduce the growth stress profile in the section (eq. 19). In the next part, we will see how the allometric coefficients can be obtained from realistic growth data.

Realistic growth data

Tree material

Numerical experiments were carried out using two reference models: one softwood *Pinus Pinaster* and one hardwood *Prunus avium* (Fig 2). Both their architectures follow Rauh's model, meaning that the branching is rythmic, the axes monopodial and the branches orthotropic [Hallé et al. (1978)]. The digital trees were computed with AMAPSim software [Barczi et al. (2007)]. Architectural parameters were obtained by observations and field studies: Coudurier et al. (1993) and Heuret et al. (2006) for *Pinus pinaster*, Caraglio (1996) and Barthélémy et al. (2009) for *Prunus avium*.

(a) (b)

Figure 2: AMAPSim representation of aerial architecture of 50 year old birch (a) and pine (b) tree.

Loading scenarii: allometric laws

The tree is composed of axes organised hierarchically according to their order: 1 for the tree seed, 2 for the trunk, 3 for the main branches, 4 for those attached to them, and so on. Each axis is described as a succession of growth units (GU), which are sections of cones, identified by a number (in order of appearance), and defined by a parent number, an order, a start and end diameter, the coordinates of the centres of both initial and final sections as well as their length (Fig 3). Note that the description provided by AmapSim does not include the internal structure of the growth units, such as eccentricity. To avoid unnecessary complications, the coordinate of the centres will be taken as those of the pith. From the model data, moments and normal force in each growth unit at any time of the tree's existence can be computed. Each unit is subjected, in addition to a part of its own weight, to that of its offsprings - this term referring to any growth unit that would fall if the studied one was cut. The normal force $\overrightarrow{N_n}$ and bending moment $\overrightarrow{M_n}$ supported by the growth unit n can be written:

$$\overrightarrow{N_n} = \frac{1}{2} m_n \vec{g} + \sum_{\substack{k \succ n \\ k\ offspring}} m_k \vec{g} \tag{22}$$

$$\overrightarrow{M_n} = \overrightarrow{G_n G'_n} \wedge \left(\frac{1}{2} m_n \vec{g} \right) + \sum_{\substack{k \succ n \\ k\ children}} \overrightarrow{G_n G_k} \wedge (m_k \vec{g}) \tag{23}$$

with G_n the centre of gravity of the current growth unit, G'_n that of is second half, on the downstream side of G_n, G_k that of an offpring of number $k > n$, m_i the mass of growth unit i and $\vec{g}$ the gravity vector. Once $\overrightarrow{N_n}$ and $\overrightarrow{M_n}$ are calculated, in the absolute coordinates used for the description of the whole tree, they are projected in the local coordinate system $(\vec{x'}, \vec{y'}, \vec{z})$, with $\vec{z}$ of the chosen cross section. In the following, in accordance with the development of the previous section, N_z will refer to the projection of $\overrightarrow{N}$ on $\vec{z}$ and M_y to that of $\overrightarrow{M}$ on $\vec{y'}$.

Power law regressions were performed to recover the allometric coefficients $\lambda_M, \lambda_N, \nu_N, \nu_M$. A summary of the analysis process is proposed in Figure 3.

Branches need to have a long loading history to exhibit interesting stress profiles. Thus, only branches of order 3 (attached to the trunk) and older than 15 (resp. 17) years were selected in *Pinus pinaster* (resp. *Prunus avium*). Finally, 64 axes for pine and 65 for cherry wood were identified. The distribution of all allometric coefficients, for the growth unit closest to the trunk, are presented in Figure 4. In *Pinus*, there is a large variation in $\nu-$coefficient, with ν_M varying by almost a factor 2 in the studied sample, indicating very variable secondary growth kinetics. In *Prunus*, the range of variation of the allometric power coefficients is smaller, which depicts a higher homogeneity of secondary growth kinetics. For both species, a great diversity in $\lambda-$ coefficients is observed, which depicts a significant variability in the loading history. This is particularly interesting as the branches show geometric determinants that do not vary over large ranges. For example, the radii of the axes considered in *Pinus* vary by only 1.5 cm between the smallest and largest axis, while the length varies by 20% between the shortest and longest axes. This reflects the complexity of predicting the loading of a branch from the determinants of the main axis, and shows the importance of branching. In both cases, these variations in the $\lambda-$coefficients result in a factor of 4 in the bending load between the lightly loaded and the heavily loaded branches.

The average values of each allometric and final geometry, indicated in table 1, will be used for the simulations.

Material data and stem orientation

The stress values in the normal wood were fixed according to the average maturation strains advised by Thibaut and Gril (2021). Similarly, the green wood MOE were given by the correlation between dry and

(a)

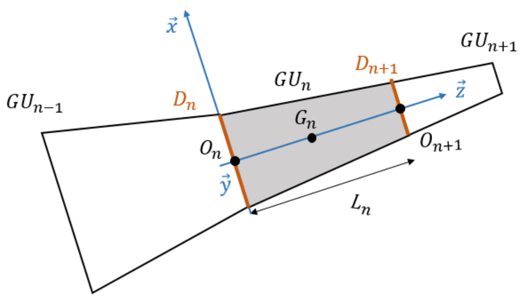

(b)

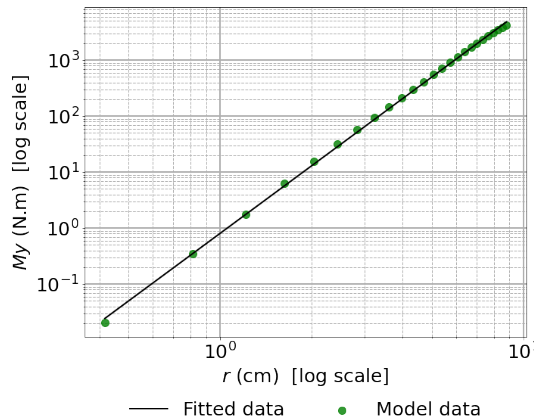

(c)

Figure 3: *Prunus avium.* Allometric law. From the geometry of the modeled branche a) and b), the bending moment is calculated. Graph c), The relationship between the branch diameter and the bending moment is plotted. The computation of the fitted curve provides the allometric law.

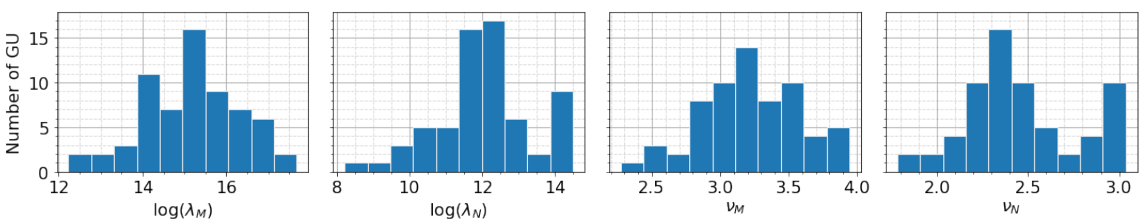

(a)

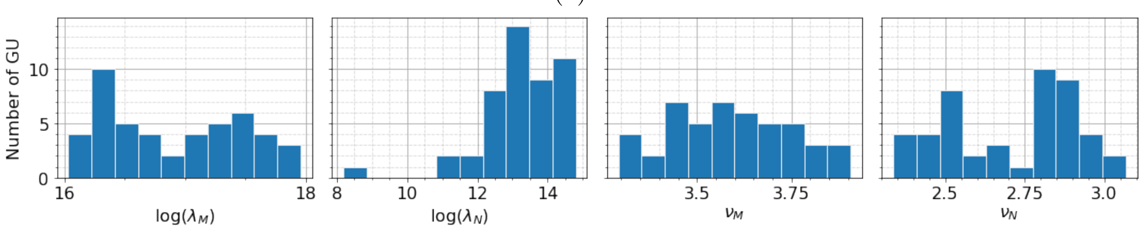

(b)

Figure 4: Statistical distribution of allometric coefficients for modelled branches: (a) Pinus branches over 15 years old; (b) Prunus branches over 17 years old. $\lambda_{M,N}$ refers to the weight, $\nu_{M,N}$ to the kinetic of secondary growth.

green MOE identified by Thibaut and Gril (2021): $Eg = 0.89 * Ed$. Dry MOE were provided by the tropix database of CIRAD [Gérard et al. (2011)]. The density of green wood was approximated by the density of water $\rho = 1000\ kg.m^{-3}$. These inputs are summarised in Table 1.

In the following section, the case of stationary growth ($\nu_b = 0$) will be considered principally and analysed thoroughly. Situations of changing curvature will be then considered briefly.

Species	λ_M $(N.m^{-\nu_M})$	λ_N $(N.m^{-\nu_N})$	ν_M	ν_N	r (cm)	μ_{NW} (μstrain)	E_d (GPa)	E_g (GPa)
Pinus pinae	-6.4e6	5e4	3.2	2.5	5	410	8.8	7.9
Prunus avium	-2.6e7	9.5e3	3.6	2.7	8	712	10.2	9.1

Table 1: Mean input characteristics of the branches

Results and discussion

Prunus avium: heavily loaded hardwood

Several postural control scenarii have been computed. First, the ability of the branch to maintain its orientation through RW formation only (Fig 5.a-c) or secondary growth eccentricity only (Fig 5.d-f) is evaluated. Then, combinations of these strategies ~~is~~ proposed (Fig 6): for each combination, one parameter (growth eccentricity or maturation) is assumed to be uniform throughout the growth of the branch, while the other is assumed to be the driver of orientation control.

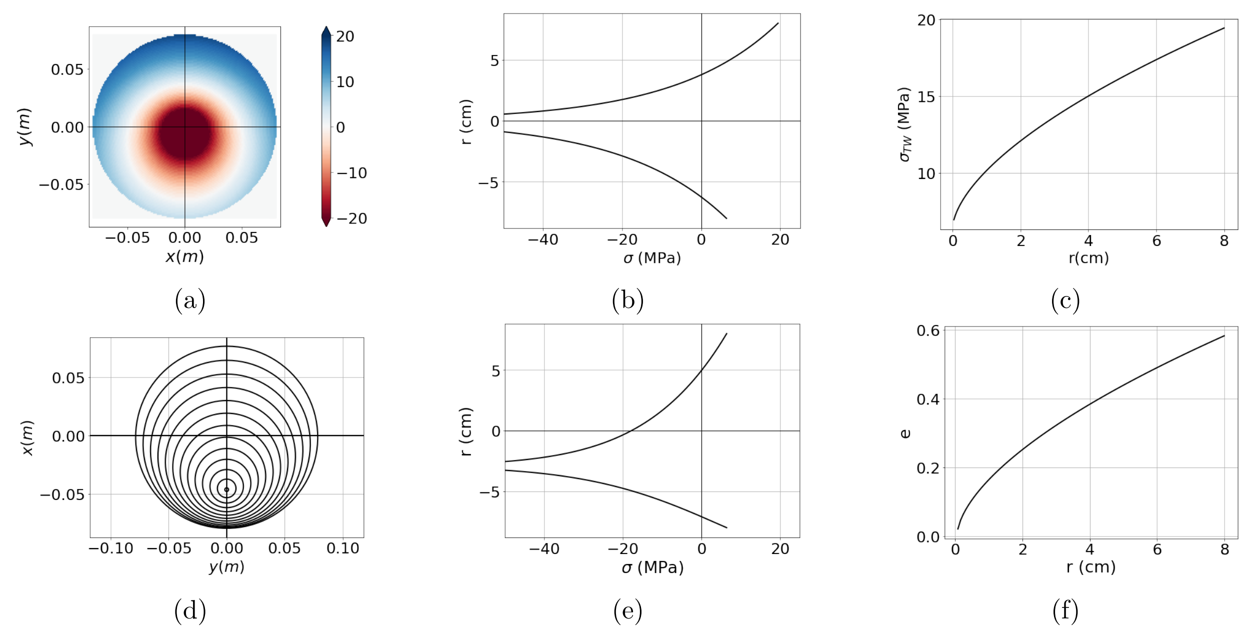

Figure 5: *Prunus avium*: Horizontal orientation maintained by the two different drivers: a-c) maturation stress and d-f) eccentricity. Different types of representation are proposed: a) (resp. d)) 2D visualisation of the growth stress (resp. eccentricity) in the whole section. b) and e) Growth stress profile on the line y=0. c) and f) Parametric representation of the tropic driver: maturation stress and eccentricity.

Both strategies alone (Fig.5) lead to realistic orders of magnitude (except near the pith, which is an intrinsic limit of our model; this specific point is discussed in section *Limits of the model*). Across the chosen combinations, no single strategy seems to be more efficient than the other. For example, eccentricity alone (5.a-c and 6.b, solid line) may be sufficient to maintain the branch orientation while keeping a sufficient mechanical safety margin ($\max(e) = 0.6$). In comparison, with zero eccentricity (Fig.6.a, dashed line), TW alone leads to a tensile strain $\mu_{RW} \approx 2140\mu$strain ($\sigma_{TW} \approx 19.5$ MPa), also far from limits observed in literature [Huang et al. (2005); Thibaut and Gril (2021)]. Moreover, eccentricity and deformation in TW acts as an optimisation of branch control and resistance to breakage: promoting epitrophic eccentricity (more radial growth on the upper side) allows less tension in TW: the more space eccentricity leaves to

TW, the lower the stress in it. Interestingly, the worst case (hypotrophic eccentricity, more radial growth on the lower side, solid line in Fig 6.a) leads to orders of magnitude that are on the border of limits, but observable: $\mu_{RW} \approx 4970\mu$strain ($\sigma_{TW} \approx 45.4$ MPa). Note that although for softwoods, there is a consensus on the eccentricity orientation (hypotrophic) for tropism responses [Timell (1986)], hardwood species can show eccentricities in both directions [Kucera and Philipson (1977); Wang et al. (2009); Tsai et al. (2012)]. The hypotrophic eccentricity (Fig 6.a) is obviously not motivated by an optimisation of postural control, suggesting the existence of trade-offs with other vital functions.
Even if the observation is the same (epitrophic eccentricity lead to less intense TW), graphs 6.b (dashed and dotted lines) show profiles that have higher safety margins than those in Figure 6.a. When combined, it seems more efficient to vary the eccentricity and keep a constant difference of maturation stress than to keep a uniform eccentricity and to vary the maturation stress. To date, there is no study that has attempted to investigate the variations in space and time of the eccentricity in the branches. This is a very interesting perspective to understand the interaction between eccentricity, maturation and postural control of inclined axes.

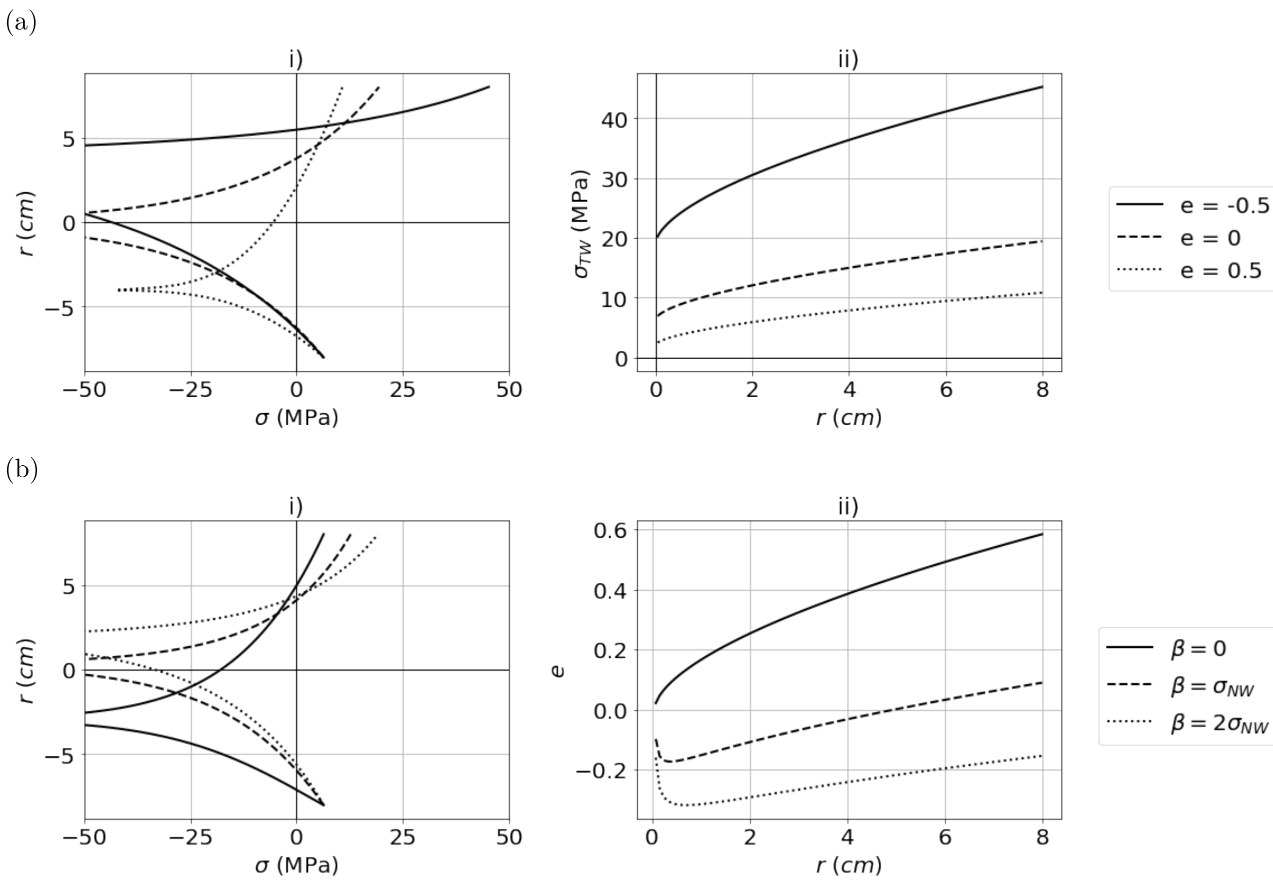

Figure 6: Illustration of different straightening strategies for *Prunus avium*: (a) constant eccentricity, the maturation is the main driver of postural control; (b)constant difference of maturation stress, the eccentricity is the main driver of postural control.

Pinus pinaster: lightly loaded softwood

Similarly, for *Pinus pinaster*, we compare the ability of maturation process alone (Fig 7.a-c) and growth eccentricity alone (Fig 7.d-f) to maintain a constant orientation, then study the combination of these processes (Figure 8). Note that the average bending moment due to weight is much higher for birch tree, by a factor roughly 10, than for pine (see λ_M and λ_N in Table 1). This may explain why the

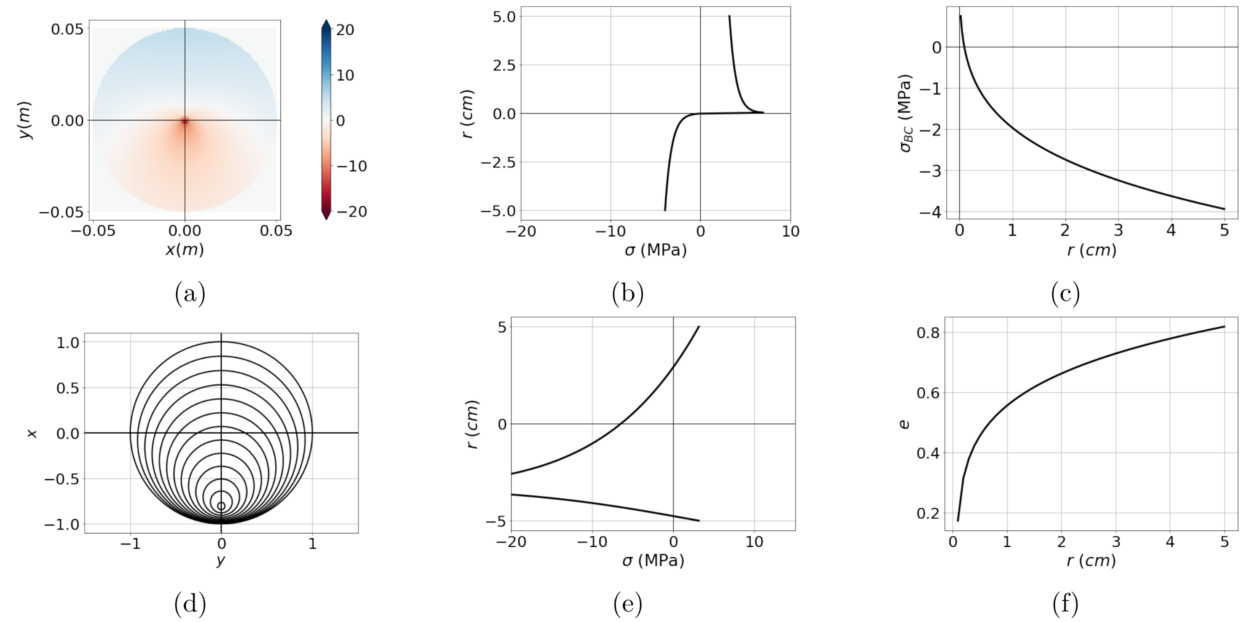

Figure 7: *Pinus pinaster*: Horizontal orientation maintained by the two different drivers: a-c) maturation stress and d-f) eccentricity. Different types of representation are proposed: a) (resp. d)) 2D visualisation of the growth stress (resp. eccentricity) in the whole section. b) and e) Growth stress profile on the line y=0. c) and f) Parametric representation of the tropic driver: maturation stress and eccentricity.

straightening drivers are much less triggered in the case of this pine. Moreover, in the current model the Young's modulus is supposed to be uniform in the whole cross section. While this hypothesis does not have much impact on the stress profiles for hardwoods, where both TW and NW produce tensile stress and the difference of Young's moduli is moderate, it modifies the results for softwoods much more. Indeed, although CW of softwoods is typically denser than NW, due to the higher inclination of cellulose microfibrils, its Young's modulus is often much lower. This explains for a part the commonly observed association of CW production with eccentric growth. This is an important limitation of the proposed formulation and will have to be kept in mind when discussing the results.

The analysis of each strategy alone (maturation: Fig 7.a-c and Fig.8.a dashed line; eccentricity: Fig 7.d-f and Fig.8.b solid line) suggests that maturation is more efficient than eccentricity. To ensure the same growth scenario, the eccentricity alone rises to about 0.8, which is not far from a limit value, whereas maturation alone leads to low maturation strains in CW (<500 μstrain, corresponding to 4 MPa). Besides, this eccentricity is not in the direction of what is commonly observed. This point remains logical, because without CW, the epitrophic eccentricity leads to shifting the bending centre upward to limit the bending moment load. Finding an eccentricity opposite to the usual one observed is therefore quite plausible. In fact, the eccentricity in the early stages of development generates a coordination problem, especially for softwoods. For hardwoods, the simultaneous building of TW and eccentricity is not an issue, whereas building a hypotrophic growth pattern without CW is not efficient for softwoods.

In case of combined effects, although eccentricity alone ensures stationarity, it does not succeed anymore when combined to a uniform maturation (red dotted line in Fig. 8.b). For the chosen parameters, this means that if the maturation strain was higher than -180 μstrain ($\sigma_{CW} \approx 1.4$ MPa, black dotted line in Fig. 8.b) the branch could not ensure its orientation using the eccentricity process only. As said before, the early stages of development in softwood seems to generate coordination problem. Finally, varying the eccentricity while keeping the maturation stress constant seems to be an irrelevant biomechanical strategy for the branch. Beyond this result, one can also wonder if this case was realistic: to what extent are there

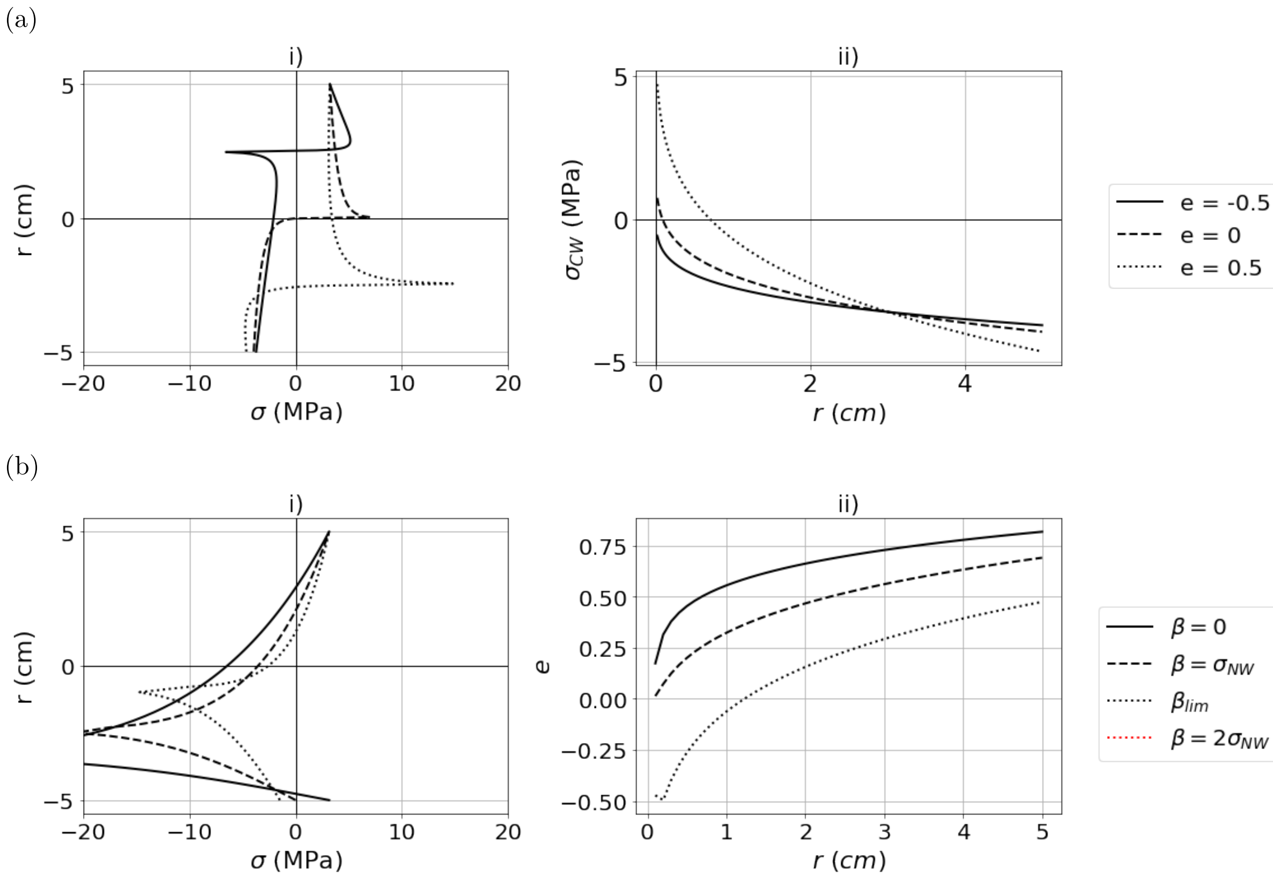

Figure 8: Illustration of different straightening strategies for textitPinus pinaster: (a) constant eccentricity, the maturation is the main driver of postural control; (b): constant maturation gradient, the eccentricity is the main driver of postural control.

constant maturation constraints throughout the growth of the branches? But if these situations do really exist, then eccentricity clearly does not have a crucial role in maintaining postural control.

For the other combined effects, the eccentricity does not bring much change in the value of the maturation stress (Fig. 8.a). However, it considerably modifies the shape of the resulting stress profiles (Fig.8.a.i). Indeed, these profiles can become 'crenellated' (Fig.8.a.i, dashed curve for zero eccentricity, solide curve for $e = -0.5$) or include tension at the pith (dotted line for $e = 0.5$). These two particular patterns are represented in the whole section in Fig. 9. It seems that before producing tension at the pith, an optimal configuration can be reached by generating compression below the pith and tension above. Ideally, this may be what each branch should tend to do. These results about the branches mechanical strategies should be compared with experimental measurements. Otherwise, theses changes of patterns could also be an optimisation of the residual strength of wood: CW is known to have better compressive strength conferred by its high lignin content and cell wall structure. Generating some tension at the pith allows the branch to create more CW. To answer this question correctly, it would be necessary to build a fracture model and to include it to our stress computation model. For example, adding an damage-elastoplastic law would allow to study the effects of stress relaxation and to understand how some profiles that are not optimal for straightening can possibly be optimal for resisting breakage.

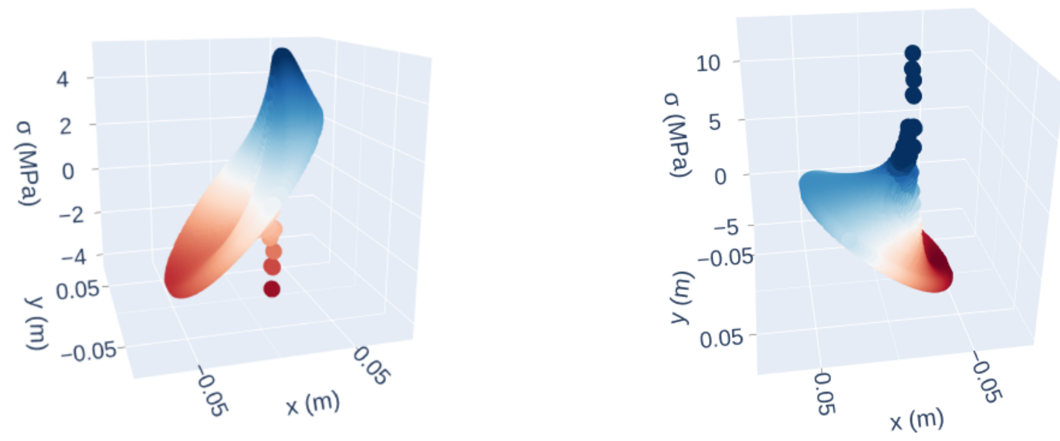

(a) ’Crenellated’ pattern

(b) Pattern with tension near the pith

Figure 9: Spatial distribution of stress in two particular cases in *Pinus pinaster*. a): Case of a uniform epitrophic eccentricity : $e = -0.5$ b). Case of a uniform hypotrophic eccentricity $e = 0.5$. Other input parameters are the same as in Fig 8.

Influence of the orientation of the branch: the stationary hypothesis

In order to evaluate the relevance of the stationarity hypothesis, different growth scenarios are considered. For each branch, the case of active straightening or passive bending is modelled. Passive bending is driven by increasing weight. Up-righting is driven by the maturation gradient, which is set at 400 μstrain ($\sigma \approx 3.2$ MPa)for pine and 700 μstrain ($\sigma \approx 6.2$ MPa) for birch tree (the gradient is of the order of magnitude of NW stress). The results are shown in Figure 10. In birch, no major change of the stress pattern is observed. In contrast, the pattern changes greatly for pine. For a passive-bending branch, a ’V’ profile and the absence of CW are observed . For straightening, the previously-mentioned profile with tension at the pith is observed. In both cases, the orders of magnitude are compatible with a mechanical safety margin for the branches. Apart from modified tropisms (change of light environment, weight change by loss of part of the branch, etc.), the maintaining of the orientation is quite common for real branches. The simulations suggest, however, that if for any reason they need to modify their orientation, they can do it without taking too much mechanical risk. The hypothesis of branch direction stationarity is totally in accordance with the long term mechanical requirements needed during the building of branches.

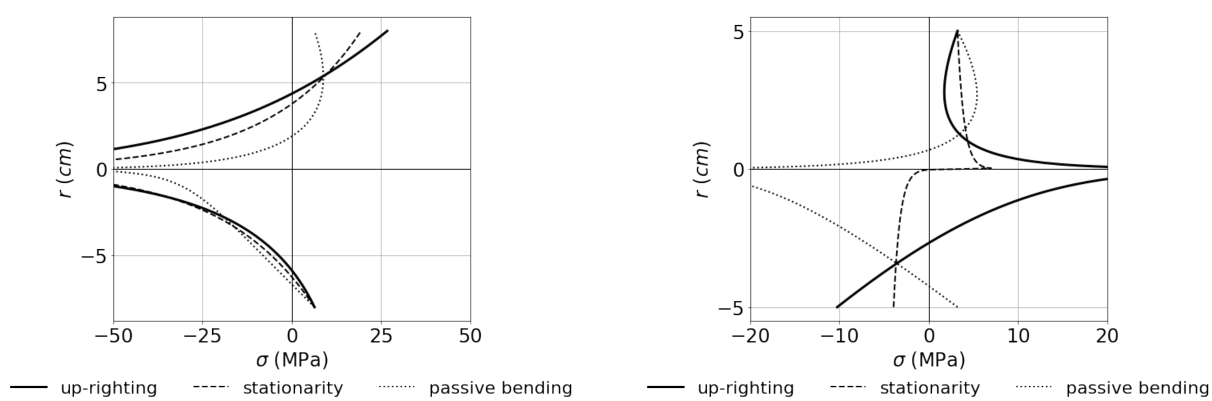

(a) Prunus

(b) Pinus

Figure 10: Distribution of growth stresses for different orientation scenarios.

About the hypothesis of the preponderance of the vertical bending moment over the horizontal bending and torsion moments

One of the initial hypothesis of our model was that the vertical bending moment (M_y in our formalism) prevails over the torsional moment M_z and horizontal bending moment M_x. This allowed to consider only one direction of eccentricity and to avoid all the non-linear terms generated by the torsional components. We evaluated the maximum values of the three moments for all modeled branches of each species for comparison purpose. The results are presented in figure 11. They enlighten that for every comparison, the vertical moment shows much higher values than the torsional and horizontal bending moments and validates our initial hypothesis.

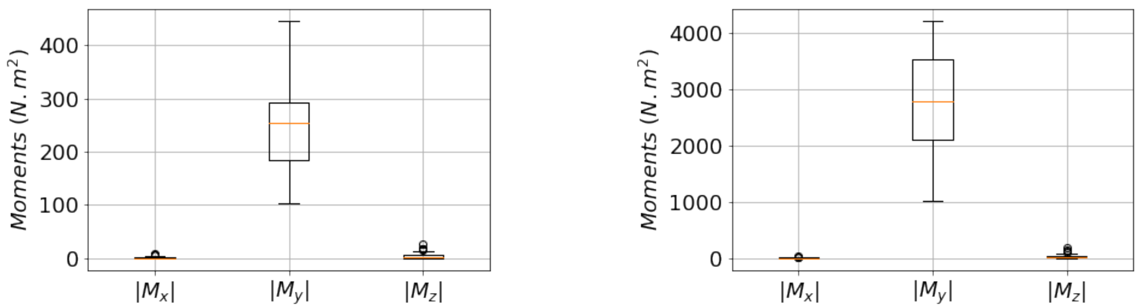

(a) Pinus

(b) Prunus

Figure 11: Comparison of maximum moments for modeled branches. Mx: horizontal moment; My: vertical moment; Mz: torsional moment.

Limits of the model

The evaluation of the stress during the first stages of stem development is an issue of the model. In almost every stress profiles, at the pith a tension or compression peak is obtained, generally exceeding wood strength, which is not compatible with branch sustainability. This point could be corrected in two ways. First, the role of the bark could be taken into account. Its mechanical role for small axes has already been studied and its importance in postural straightening was clearly highlighted [Clair et al. (2019); Ghislain et al. (2019)]. Our model could include the mechanical action of bark in the early stages of branch development. This improvement would require additional data about the mechanical behaviour of the bark but would bring more realistic stress predictions and limit the artefacts at the pith. A second exciting perspective would be to take into account the elastoplastic behaviour of wood. By imposing a realistic plastic strain limit, the peak at the pith would then disappear; and the increments would be spread over the middle part of the section, thus modifying the odd pattern observed in figure 9.

A another limit is the hypothesis about wood stiffness. It is particularly unfavourable for softwoods, because it reinforces some geometric phenomena (see the one in Fig.8.a.i). In this context, it would be very interesting to evaluate the potential link between eccentricity and modulus variations. If the latter is established, the eccentricity that we would impose with the model would serve to compensate or amplify the effect of the tension wood. However, it remains unclear whether or not this would explain the limited action available to the branch in the case of a constant maturation stress.

Finally, modelling the evolution of normal force and bending moment loads by allometric laws is not optimal. Indeed, the orientation of the branch changes with time, and implies variations of the effect of weight. Modelling a constant increase of the normal force is inappropriate if the inclination of the branch decreases with time. An improvement of the model could be the construction of loads based on equivalent length allometries taking into account the mass of the branch, and the computation of the loads for each position in the right reference frame.

Conclusion and perspectives

A semi-analytical growth stress model has been developed a in the context of branch development. At each radius increment, the stress balance is computed in order to fit with a given curvature. A first novelty of this model is that it takes into account the role of the eccentricity variation in time. A second contribution is that it computes the stress distribution in the whole cross-section. It has been applied to test the effectiveness of two well-known biomechanical strategies of woody plants to control the orientation of their stem: secondary growth eccentricity and reaction wood formation. The case of softwood and hardwood branches were computed using digital data provided by AMAPSim software. For hardwood, growth stress simulations show that both strategies are efficient to maintain a given orientation, although eccentricity is more so than the generation of maturation gradients. On the contrary, in the case of softwood, reaction wood formation appears to be more efficient than eccentric growth. Obviously, in all cases, the combination of both processes yields very high stress levels that are able to keep the branch straight or modify its orientation. Few strategies, such as forming reaction wood uniformly over time while allowing eccentric growth, are not optimal to maintain the orientation. However, since growth eccentricity does not play a major role in straightening capabilities, it does not influence much the shape of the stress profiles. Few odd and critical profiles "in crenelated" or "with traction" near the pith have been identified. Their analysis provides very exciting perspectives for further experimental works in order to get real data. Finally, for lightly loaded softwood branches, the eccentric growth plays a minor role in straightening. The model is limited in terms of predicting capacity because of the lack of experimental data.

Now that a complete model is available, it becomes crucial to start experimental investigations in order to compare the outputs with real in situ observations. Especially, we need to evaluate the relevance of the different scenarii (constant gradient, constant eccentricity). The question of the relevance of the stationarity of the branch's trajectory hypothesis has been also established. In particular, we have shown that the branch could deviate from a stationary trajectory without limiting its mechanical strength too much.

A key point for understanding branch sizing is the question of biomass costs. Building additional wood on one side or forming reaction wood are carbon sinks with possible trade-offs. One perspective of work would be to affect a cost to the production of reaction wood as well as to eccentric growth. The resulting computations could then help to understand the choice of some strategies over others and would lead to coupling the biomechanical point of view to other biological considerations.

References

T. Alméras, D. Jullien, and J. Gril. *Modelling, Evaluation and Biomechanical Consequences of Growth Stress Profiles Inside Tree Stems*, pages 21–48. Springer International Publishing, Cham, 2018. ISBN 978-3-319-79099-2. doi: 10.1007/978-3-319-79099-2_2. URL `https://doi.org/10.1007/978-3-319-79099-2_2`.

T. Alméras and B. Clair. Critical review on the mechanisms of maturation stress generation in trees. *Journal of The Royal Society Interface*, 13(122):20160550, 2016. doi: 10.1098/rsif.2016.0550. URL `https://royalsocietypublishing.org/doi/abs/10.1098/rsif.2016.0550`.

T. Alméras and M. Fournier. Biomechanical design and long-term stability of trees: Morphological and wood traits involved in the balance between weight increase and the gravitropic reaction. *Journal of Theoretical Biology*, 256(3):370–381, 2009. ISSN 0022-5193. URL `http://www.sciencedirect.com/science/article/pii/S0022519308005389`.

T. Alméras, A. Thibaut, and J. Gril. Effect of circumferential heterogeneity of wood maturation strain, modulus of elasticity and radial growth on the regulation of stem orientation in trees. *Trees*, 19(4): 457–467, 2005. ISSN 1432-2285. URL `https://doi.org/10.1007/s00468-005-0407-6`.

P. Ancelin, T. Fourcaud, and P. Lac. Modelling the biomechanical behaviour of growing trees at the forest stand scale. part i: Development of an incremental transfer matrix method and application to simplified tree structures. *Annals of Forest Science*, 61(3):263–275, 2004.

R. R. Archer. On the distribution of tree growth stresses. ii. stresses due to asymmetric growth strains. *Wood Science and Technology*, V10:293–309, 1976.

R. R. Archer and F. E. Byrnes. On the distribution of tree growth stresses – part i: An anisotropic plane strain theory. *Wood Science and Technology*, 8(3):184–196, 1974. ISSN 1432-5225. URL `https://doi.org/10.1007/BF00352022`.

J.-F. Barczi, H. Rey, Y. Caraglio, P. de Reffye, D. Barthélémy, Q. X. Dong, and T. Fourcaud. AmapSim: A Structural Whole-plant Simulator Based on Botanical Knowledge and Designed to Host External Functional Models. *Annals of Botany*, 101(8):1125–1138, 09 2007. ISSN 0305-7364. doi: 10.1093/aob/mcm194. URL `https://doi.org/10.1093/aob/mcm194`.

D. Barthélémy, Y. Caraglio, and S. Sabatier. 4.1 crown architecture of valuable broadleaved species. *Valuable broadleaved forests in Europe*, 22:87, 2009.

D. Barthélémy and Y. Caraglio. Plant Architecture: A Dynamic, Multilevel and Comprehensive Approach to Plant Form, Structure and Ontogeny. *Annals of Botany*, 99(3):375–407, 01 2007. ISSN 0305-7364. doi: 10.1093/aob/mcl260. URL `https://doi.org/10.1093/aob/mcl260`.

Y. Caraglio. Le développement architectural du merisier. *Forêt Entreprise 107*, (107):72–80, 1996.

B. Clair, B. Ghislain, J. Prunier, R. Lehnebach, J. Beauchêne, and T. Alméras. Mechanical contribution of secondary phloem to postural control in trees: the bark side of the force. *New Phytologist*, 221(1): 209–217, 2019. doi: https://doi.org/10.1111/nph.15375. URL `https://nph.onlinelibrary.wiley.com/doi/abs/10.1111/nph.15375`.

T. Coudurier, D. Barthelemy, B. Chanson, F. Courdier, and C. Loup. Premier résultats sur la modélisation du pin maritime pinus pinaster ait.(pinecae). *Architecture des arbres fruitiers et forestiers*, page 306, 1993.

C. Coutand, M. Fournier, and B. Moulia. The gravitropic response of poplar trunks: Key roles of prestressed wood regulation and the relative kinetics of cambial growth versus wood maturation. *Plant Physiology*, 144(2):1166–1180, 2007. ISSN 0032-0889. doi: 10.1104/pp.106.088153. URL `http://www.plantphysiol.org/content/144/2/1166`.

J. B. Fisher and J. W. Stevenson. Occurrence of reaction wood in branches of dicotyledons and its role in tree architecture. *Botanical Gazette*, 142(1):82–95, 1981. doi: 10.1086/337199. URL `https://doi.org/10.1086/337199`.

T. Fourcaud, F. Blaise, P. Lac, P. Castéra, and P. de Reffye. Numerical modelling of shape regulation and growth stresses in trees. *Trees*, 17(1):31–39, 2003. ISSN 1432-2285. URL `https://doi.org/10.1007/s00468-002-0203-5`.

M. Fournier, B. Chanson, D. Guitard, and B. Thibault. Mécanique de l'arbre sur pied : modélisation d'une structure en croissance soumise à des chargementspermanents et évolutifs. 1. analyse des contraintes de support. 1991a.

M. Fournier, B. Chanson, D. Guitard, and B. Thibault. Mécanique del'arbre sur pied :modélisation d'une structure en croissance soumise à des chargements permanents et évolutifs.2. analyse tridimensionnelle des contraintesde maturation, cas du feuillu standard. 1991b.

M. Fournier, H. Baillères, and B. Chanson. Tree biomechanics : growth, cumulative prestresses, and reorientations. *Biomimetics*, 2(3):229–251, 1994.

B. Ghislain, T. Alméras, J. Prunier, and B. Clair. Contributions of bark and tension wood and role of the g-layer lignification in the gravitropic movements of 21 tropical tree species. *Annals of Forest Science*, 76(4):107, 2019. ISSN 1297-966X. URL https://doi.org/10.1007/s13595-019-0899-7.

J. Gérard, D. Guibal, S. Paradis, M. Vernay, J. Beauchêne, L. Brancheriau, I. Châlon, C. Daigremont, P. Détienne, D. Fouquet, P. Langbour, S. Lotte, M.-F. Thévenon, C. Méjean, and A. Thibaut. Tropix 7, 2011. URL http://tropix.cirad.fr/en.

F. Hallé, R. A. Oldeman, and P. B. Tomlinson. *Tropical trees and forests: an architectural analysis*. Springer Verlag, 1978.

P. Heuret, C. Meredieu, T. Coudurier, F. Courdier, and D. Barthélémy. Ontogenetic trends in the morphological features of main stem annual shoots of pinus pinaster (pinaceae). *American Journal of Botany*, 93(11):1577–1587, 2006. doi: https://doi.org/10.3732/ajb.93.11.1577. URL https://bsapubs.onlinelibrary.wiley.com/doi/abs/10.3732/ajb.93.11.1577.

Y.-S. Huang, S.-S. Chen, L.-L. Kuo-Huang, and C.-M. Lee. Growth strain in the trunk and branches of chamaecyparis formosensis and its influence on tree form. *Tree Physiol*, 25(9):1119–1126, Sept. 2005. ISSN 0829-318X. URL https://doi.org/10.1093/treephys/25.9.1119.

Y.-S. Huang, L.-F. Hung, and L.-L. Kuo-Huang. Biomechanical modeling of gravitropic response of branches: roles of asymmetric periphery growth strain versus self-weight bending effect. *Trees*, 24(6):1151–1161, 2010. ISSN 1432-2285. URL https://doi.org/10.1007/s00468-010-0491-0.

L.-F. Hung, C.-C. Tsai, S.-J. Chen, Y.-S. Huang, and L.-L. Kuo-Huang. Study of tension wood in the artificially inclined seedlings of koelreuteria henryi dummer and its biomechanical function of negative gravitropism. *Trees*, 30(3):609–625, 2016. ISSN 1432-2285. URL https://doi.org/10.1007/s00468-015-1304-2.

L.-F. Hung, C.-C. Tsai, S.-J. Chen, Y.-S. Huang, and L.-L. Kuo-Huang. Strain distribution, growth eccentricity, and tension wood distribution in the plagiotropic and orthotropic branches of koelreuteria henryi dummer. *Trees*, 31(1):149–164, 2017. ISSN 1432-2285. URL https://doi.org/10.1007/s00468-016-1464-8.

L. J. Kucera and W. R. Philipson. Growth eccentricity and reaction anatomy in branchwood of drimys winteri and five native new zealand trees. *New Zealand Journal of Botany*, 15(3):517–524, 1977. doi: 10.1080/0028825X.1977.10429625. URL https://doi.org/10.1080/0028825X.1977.10429625.

H. Kübler. Studien über wachstumsspannungen des holzes iii. längenänderungen bei der wärmebehandlung frishen holzes. *Holz Rohst Werkst*, 17(3):77–86, 1959.

J. E. Nicholson. A rapid method for estimating longitudinal growth stresses in logs. *Wood Science and Technology*, 5(1):40–48, 1971. ISSN 1432-5225. URL https://doi.org/10.1007/BF00363119.

B. Thibaut. Three-dimensional printing, muscles, and skeleton: mechanical functions of living wood. *Journal of Experimental Botany*, 70(14):3453–3466, 04 2019. ISSN 0022-0957. doi: 10.1093/jxb/erz153. URL https://doi.org/10.1093/jxb/erz153.

B. Thibaut and J. Gril. Tree growth forces and wood properties. *Peer Community Journal*, 1:e46, 2021. doi: 10.24072/pcjournal.48. URL https://peercommunityjournal.org/articles/10.24072/pcjournal.48/.

T. E. Timell. *Compression wood in gymnosperms*, volume 1. Springer, 1986.

C.-C. Tsai, L.-F. Hung, C.-T. Chien, S.-J. Chen, Y.-S. Huang, and L.-L. Kuo-Huang. Biomechanical features of eccentric cambial growth and reaction wood formation in broadleaf tree branches. *Trees*, 26(5):1585–1595, 2012. ISSN 1432-2285. URL https://doi.org/10.1007/s00468-012-0733-4.

Y. Wang, J. Gril, and J. Sugiyama. Is the branch of viburnum odoratissimum var. awabuki reaction wood? unusual eccentric growth and various distributions of growth strain. In *6th Plant Biomechanics Conference*, pages 328–334, 2009.

H. Yamamoto, M. Yoshida, and T. Okuyama. Growth stress controls negative gravitropism in woody plant stems. *Planta*, 216(2):280–292, 2002. ISSN 1432-2048. URL https://doi.org/10.1007/s00425-002-0846-x.

J. L. Yang, H. Baillères, T. Okuyama, A. Muneri, and G. Downes. Measurement methods for longitudinal surface strain in trees: a review. *Australian Forestry*, 68(1):34–43, 2005. doi: 10.1080/00049158.2005.10676224. URL https://doi.org/10.1080/00049158.2005.10676224.

M. Yoshida and T. Okuyama:. Techniques for measuring growth stress on the xylem surface using strain and dial gauges. 56(5):461–467, 2002. doi: doi:10.1515/HF.2002.071. URL https://doi.org/10.1515/HF.2002.071.

Appendix A

The calculation of integrals of the system 3 needs some preliminary elements. The situation of two consecutive rings is represented in figure 12. Each position x in the geometrical reference frame is expressed with respect to the position x' in the pith reference frame according to the equation:

$$x = r\cos\theta = x' - \bar{e}R \tag{24}$$

with r the radius at time t and R the radius at the final time.

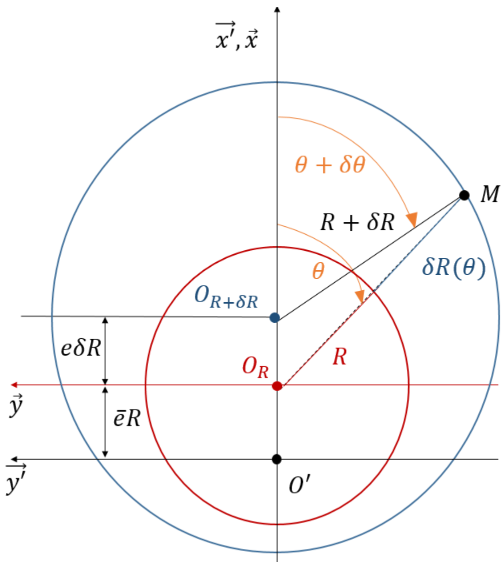

Figure 12: Representation of two consecutive rings and the elements needed to calculate $\delta R(\theta)$

Then, the integrals of the system 3 are computed as follows:

$$\begin{aligned}
\int_s \delta\sigma ds &= \int_s E\left[\delta a + (x + \bar{e}.R)\delta b\right] r\delta r d\theta \\
&= E\pi R^2\left(\delta a + \bar{e}.R\delta b\right) \\
\int_s x'\delta\sigma ds &= \int_s \left[\delta a + (x + \bar{e}.R)\delta b\right]\left[x + \bar{e}.R\right] r\delta r d\theta \\
&= E\pi R^3\left[\bar{e}\delta a + R\left(\bar{e}^2 + \frac{1}{4}\right)\delta b\right]
\end{aligned}$$

The tangential distribution of the radius increment $\delta R(\theta)$ are required in order to compute the terms of maturation. The Figure 12, enlighten that $\overrightarrow{OM} + \overrightarrow{MO'} = \overrightarrow{OO'}$:

$$\begin{cases}
[R + \delta R(\theta)]\cos\theta - (R + \delta R)\cos(\theta + \delta\theta) = e_R\delta R & \text{(25a)} \\
[R + \delta R(\theta)]\sin\theta - (R + \delta R)\sin(\theta + \delta\theta) = 0 & \text{(25b)}
\end{cases}$$

By setting $\delta\theta \to 0$, it comes:

$$\begin{cases}
\cos(\theta + \delta\theta) = \cos\theta - \sin\theta\delta\theta & \text{(26a)} \\
\sin(\theta + \delta\theta) = \sin\theta + \cos\theta\delta\theta & \text{(26b)}
\end{cases}$$

Substituting 26 into 25, and using the combination 25a.$\cos\theta$ + 25b.$\sin\theta$, $\delta R(\theta)$ can finally be written as:

$$\boxed{\delta R(\theta) = \delta R\left[1 + e_R \cos\theta\right]} \tag{27}$$

Then:

$$\begin{aligned}
\int_{\delta s} \sigma_0^i ds &= \int_{\delta s} \sigma_0^i(\theta) R\delta R(\theta) d\theta \\
&= \int_{\delta s} \left[\alpha + \beta\cos\theta\right]\left[1 + e\cos\theta\right] R\delta R(\theta) d\theta \\
&= \pi\left(2\alpha + e\beta\right) R\delta R \\
\int_{\delta s} x'\sigma_0^i ds &= \int_{\delta s} \sigma_0^i(\theta)(x + e.R) R\delta R(\theta) d\theta \\
&= R^2\delta R\pi\left(3\alpha e + \beta e^2 + \beta\right)
\end{aligned}$$

Appendix B

The matrix system 7 becomes:

$$\begin{cases}
\delta a = \dfrac{\delta F_0 K_2 - \delta F_1 K_1}{K_0 K_2 - K_1^2} & (28a) \\
\delta b = \dfrac{\delta F_0 K_1 - \delta F_1 K_0}{K_1^2 - K_0 K_2} & (28b)
\end{cases}$$

Then, numerators and denominators are calculated separately:

$$K_0 K_2 - K_1^2 = E^2\pi^2 R^6\left(\overline{e}^2 + \frac{1}{4}\right) - E^2\pi^2 R^6 \overline{e}^2 = \frac{\left(E\pi R^3\right)^2}{4}$$

$$\begin{aligned}
\delta F_0 K_2 - \delta F_1 K_1 &= E\pi^2 R^5\left[-\left(2\alpha + e\beta\right)\left(\overline{e}^2 + \frac{1}{4}\right) + \overline{e}\left(3\alpha e + \beta e^2 + \beta\right)\right]\delta R + E\pi R^3\left[R\delta N\left(\overline{e}^2 + \frac{1}{4}\right) + \overline{e}\delta M\right] \\
&= E\pi^2 R^5\left[\alpha\left(3e\overline{e} - 2\overline{e}^2 - \frac{1}{2}\right) + \beta\left(\overline{e}e^2 - e\overline{e}^2 + \overline{e} - \frac{e}{4}\right)\right]\delta R + E\pi R^3\left[R\delta N\left(\overline{e}^2 + \frac{1}{4}\right) + \overline{e}\delta M\right]
\end{aligned}$$

$$\begin{aligned}
\delta F_0 K_1 - \delta F_1 K_0 &= E\pi^2 R^4\left[-\overline{e}\left(2\alpha + e\beta\right) + \left(3\alpha e + e^2\beta + \beta\right)\right]\delta R + E\pi R^2\left[\overline{e}R\delta N + \delta M\right] \\
&= E\pi^2 R^4\left[\alpha\left(3e - 2\overline{e}\right) + \beta\left(1 + e^2 - e\overline{e}\right)\right]\delta R + E\pi R^2\left[\overline{e}R\delta N + \delta M\right]
\end{aligned}$$

Putting the calculations together, system 28 becomes:

$$\begin{cases}
\delta a = \dfrac{4}{ER}\left[\alpha\left(3e\overline{e} - 2\overline{e}^2 - \dfrac{1}{2}\right) + \beta\left(\overline{e}e^2 - e\overline{e}^2 + \overline{e} - \dfrac{e}{4}\right)\right]\delta R + \dfrac{4}{E\pi R^3}\left[R\delta N\left(\overline{e}^2 + \dfrac{1}{4}\right) + \overline{e}\delta M\right] \\
\delta b = \dfrac{-4}{ER^2}\left[\alpha\left(3e - 2\overline{e}\right) + \beta\left(1 + e^2 - e\overline{e}\right)\right]\delta R + \dfrac{-4}{E\pi R^4}\left[\overline{e}R\delta N + \delta M\right]
\end{cases}$$

Appendix C

The following calculus is based on Figure 3.b). To get the vertical bending moment M_y of unit n (eq 23), one need the calculation of each volume V_n and center of gravity G_n. Lets fix $D(z)$ the deflection of the cone. It comes:

$$V_n = \int_0^{L_n} \frac{\pi D(z)^2}{4} dz \tag{30}$$

where $D(z) = D_n + \left(\frac{D_{n+1}-D_n}{L_n}\right) z$. One gives

$$O_n G_n = \frac{1}{V_n} \int_0^{L_n} \frac{\pi D(z)^2}{4} z dz \tag{31}$$

Setting $\gamma = \frac{D_{n+1}-D_n}{D_n}$ and $\xi = \frac{L_n}{z}$, the equation 30 and 31 then become:

$$V_n = \frac{\pi D_n^2 L_n}{4} \int_0^1 (1+\gamma\xi)^2 \, d\xi = \frac{\pi D_n^2 L_n}{4} . \left(1 + \gamma + \frac{\gamma^2}{3}\right)$$

$$O_n G_n = \frac{1}{V_n} \frac{\pi D_n^2 L_n^2}{4} . \left(\frac{1}{2} + \frac{2\gamma}{3} + \frac{\gamma^2}{4}\right)$$

So, finally, $O_n G_n$ can be written:

$$O_n G_n = \frac{L_n}{2} \left(\frac{1 + \frac{4}{3}\gamma + \frac{1}{2}\gamma^2}{1 + \gamma + \frac{1}{3}\gamma^2}\right) \tag{32}$$